Effect of hydrolysis time on the morphological, physical, chemical, and thermal behavior of sugar palm nanocrystalline cellulose (*Arenga pinnata (Wurmb.) Merr*)

RA Ilyas[1,2], SM Sapuan[1,2] ⬤, MSN Atikah[3], MRM Asyraf[4],
S Ayu Rafiqah[2], HA Aisyah[2], N Mohd Nurazzi[5] and
MNF Norrrahim[6]

Abstract

Sugar palm nanocrystalline celluloses (SPNCCs) were isolated from sugar palm fiber (SPF). In this study, acid hydrolysis (60 wt. %) at different reaction times (30, 45, and 60 min) was carried out to investigate the optimum yield of NCC. The physical properties, degree of polymerization, chemical composition, structural analysis, crystallinity, surface area and charge, zeta potential, thermal analysis, and morphological characterization were also conducted to determine the outcome (efficiency) of the process. The results showed that a needle-like shape was observed under transmission electron microscopy (TEM) studies. TEM analysis showed optimum aspect ratios of 13.46, 14.44, and 13.13 for isolated SPNCC-I, SPNCC-II, and SPNCC-III, respectively. From thermogravimetric analysis (TGA), the degradation temperature of NCC decreased slightly from 335.15°C to 278.50°C as the reaction time increased. A shorter hydrolysis time tended to produce SPNCC with higher thermal stability, as proven in thermal analysis by TGA. The optimal isolation time was found to be around 45 min at 1200 rpm during hydrolysis at 45°C with 60% sulfuric acid. Therefore, the extracted SPNCC from SPF has huge potential to be utilized in the bionanocomposite field for the production of biopackaging, biomedical products, etc.

Keywords

hydrolysis treatment, sugar palm fiber, nanocrystalline cellulose, optimization

[1]Advanced Engineering Materials and Composites Research Centre (AEMC), Department of Mechanical and Manufacturing Engineering, Faculty of Engineering, Universiti Putra Malaysia, UPM Serdang, Selangor, Malaysia
[2]Laboratory of Biocomposite Technology, Institute of Tropical Forestry and Forest Products (INTROP), Universiti Putra Malaysia, UPM Serdang, Selangor, Malaysia
[3]Department of Chemical and Environmental Engineering, Faculty of Engineering, Universiti Putra Malaysia, UPM Serdang, Selangor, Malaysia
[4]Department of Aerospace Engineering, Faculty of Engineering, Universiti Putra Malaysia, UPM Serdang, Selangor, Malaysia
[5]AdvancedCentre for Defence Foundation Studies, National Defence University of Malaysia, Kem Sungai Besi, Kuala Lumpur, Malaysia
[6]Research Centre for Chemical Defence, National Defence University of Malaysia, Kem Sungai Besi, Kuala Lumpur, Malaysia

Corresponding authors:
SM Sapuan, Advanced Engineering Materials and Composites Research Centre (AEMC), Department of Mechanical and Manufacturing Engineering, Faculty of Engineering, Universiti Putra Malaysia, 43400 UPM Serdang, Selangor, Malaysia
Laboratory of Biocomposite Technology, Institute of Tropical Forestry and Forest Products (INTROP), Universiti Putra Malaysia, 43400 UPM, Serdang, Selangor, Malaysia
Email: sapuan@upm.edu.my
RA Ilyas, Advanced Engineering Materials and Composites Research Centre (AEMC), Department of Mechanical and Manufacturing Engineering, Faculty of Engineering, Universiti Putra Malaysia, 43400 UPM Serdang, Selangor, Malaysia
Laboratory of Biocomposite Technology, Institute of Tropical Forestry and Forest Products (INTROP), Universiti Putra Malaysia, 43400 UPM, Serdang, Selangor, Malaysia
Email: ahmadilyasrushdan@yahoo.com

In the past decades, the increasing recognition of the need to protect the Mother Nature has resulted in the growing utilization of various natural resources and eco-friendly materials for numerous applications.[1–4] Natural fibers are among the main natural resources that can be highlighted, especially in developing country like Malaysia, which has large agricultural production based on sugar palm, kenaf, palm oil, rubber, coconut, paddy, and others.[5–8] The use of biodegradable polymer-based materials has been greatly hindered by their intractable nature, poor water sensitivity, and poor mechanical strength and brittleness[9–13]; therefore, the use of natural fibers as reinforcements in bioplastic polymer composites has attracted substantial attention during the last few decades.[14–17] Various chemical and physical treatments have been tested to overcome these problems, including blending with other synthetic polymers, chemical modification, graft copolymerization, and incorporating fillers such as natural fibers, lignin, clay, sugar palm fiber (SPF), sugar palm-derived cellulose, and multi-walled carbon nanotubes.[18–22]

Natural fibers are classified based on their origins, such as animals, minerals, or plants.[23–25] Plant fibers are further categorized into subgroups according to their sources, such as seed fibers, fruit fibers, leaf fibers, and stem fibers.[26–31] According to Bledzki and Gassan,[32] the properties of natural plant fibers depend on their composition. Plant fibers are composite tissues formed by the combination of three main components: cellulose (a semicrystalline polymer), hemicellulose, and lignin (an amorphous polymer).[33–36] In the current study, cellulose acts as the most important component compared to the other two components due to its intrinsic properties, which present as a linear polymer of the poly(1,4-β-D-anhydroglucopyranose) unit. This unit is composed of hydroxyl groups that allow cellulose to form strong hydrogen bonds.[37–39] In fact, removing the amorphous region would affect the crystallinity index, surface morphological structure, and thermal stability of the subjected fibers.[40]

The critical components responsible for natural fiber stiffness are nanocrystalline celluloses (NCCs). With a width ranging from 5 to 80 nm and length from 100 to 250 nm, NCCs are highly crystalline materials formed by hydrogen bonds between hydroxyl groups and the oxygen of adjacent molecules.[41–44] With the combination of low density, high aspect ratio of 100, high mechanical strength, high surface area of $100 \, m^2 \, g^{-1}$, unique morphology, non-toxic nanofiber, high mechanical properties, high crystallinity, availability, biodegradability, and renewability, NCCs have drawn vast interest for their utilization as potential nanofillers in bionanocomposites.[45] These units are stabilized by a strong hydrogen interaction between hydroxyl groups

via intermolecular hydrogen bonding, which form an ordered structure fabricated together into compact microfibrils. Hence, in order to obtain purified NCC, hydrolysis treatment is utilized to remove amorphous polymers (i.e., hemicellulose and lignin). According to Deepa et al.,[46] the isolation of NCC has shown improvement in terms of the crystallinity and thermal stability of nanofibers. Moreover, the properties of NCC are closely related to their size, surface charge, and structure.[47–49] According to Naduparambath et al.,[50] there is a certain degree of grafting of the sulfate group on the surface of NCC during sulfuric acid (H_2SO_4) hydrolysis treatment. These groups impart a negative surface charge to NCC that stabilizes the aqueous suspension against agglomeration and compromises the thermal stability of nanocrystals.[51–53] The most common commercial natural fiber resource containing cellulose is wood; however, other non-wood plants, such as hemp, sugar palm, jute, cotton, and sisal, also contain a large amount of cellulose. Acid hydrolysis treatment is a well-known process for the isolation of NCC from cellulose macrofiber. Acid hydrolysis allows the removal of amorphous polymers of cellulose fibers under controlled conditions whilst keeping crystalline polymers intact in the form of crystalline nanofibers.[1] The preparation of NCC has used a wide range of raw materials as extractive media in the past decades. Among these raw materials, several of them have been experimented to isolate nanocellulose embedded in agro-residue plants, such as sago seed shells,[50] ginger fiber,[36] water hyacinth,[33] pistachio shells,[54] soy hulls,[55] and wheat straw.[56] The selection of natural fibers for polymer composites is important, as it affects the thermal and mechanical properties.[57–60] Pokok kabung or enau is the Malaysian name for *Arenga pinnata (Wurmb.) Merr.*, which is commonly known as black-fiber palm or sugar palm. This plant is a member of the *Palmae* family and also belongs to the subfamily of *Arecoideae* and tribe of *Caryoteae*.[26–28] In tropical countries like Malaysia, SPFs at present are by-products from sugar palm cultivation, in which the trees and fibers are left to die by sugar palm farmers after several years of harvesting its sugar palm from the sap of the trees' flower bunches. At other times, not all sugar palm trees yield sugar-rich sap, where sometimes up to half of the trees in a plantation field are unproductive. These agro-residue fibers comprise a high percentage of cellulose content (56.8 wt. %)[9] that can be used for industrial purposes, where the wastes are converted to high-value nanomaterial products, besides having huge potential to be reinforced into nanocomposite products. In addition, it is expected that selecting sugar palm fibers as low-cost NCC agro-residual sources will increase the production of nanocrystalline, as well as reducing

the production cost. This paper aims to optimize the isolation of NCC with maximum yield at optimum hydrolysis time.

Little or no investigation has been reported on the effect of hydrolysis time on the physical, chemical, morphological, physical, chemical, and thermal behavior of sugar palm nanocrystalline cellulose (SPNCC; *Arenga pinnata (Wurmb.) Merr*) based on literature studies. Hence, in the present work, NCCs embedded within sugar palm fibers were successfully isolated using H_2SO_4 hydrolysis treatment at different reaction times (30, 45, and 60 min). The prepared NCCs were characterized as to their physical, chemical, and morphological properties, as well as their chemical composition, degree of polymerization, zeta potential, yield, surface area, size distribution, crystallinity, and thermal properties.

Procedure and materials

Materials

The site that produced both sugar palm fiber (SPF) and sugar palm starch (SPS) utilized in this study is located in the city of Jempol, Negeri Sembilan, Malaysia. Chemicals such as sodium chlorite ($NaClO_2$), acetic acid (CH_3COOH), and sodium hydroxide (NaOH) were supplied by Sue Evergreen Sdn. Bhd. (Semenyih, Malaysia).

Extraction of sugar palm fiber and sugar palm-derived cellulose

SPF exists on the trunk of the sugar palm tree as a natural woven fiber that was removed by an axe as it covers the tree. Afterwards, the sampled SPF was ground in a Fritsch Pulverisette mill and screened to the preferred size of 2 mm. Delignification and mercerization processes were used for the extraction of cellulose fibers from SPF.[61,62] The preparation of holocellulose deployed the bleaching process, according to ASTM D1104-56 (1978). This initial delignification step was designed to eliminate lignin that presents in SPF. This process yielded sugar palm bleached fiber (SPBF). Then, the ASTM D1103-60 (1977) standard was used on SPBF to produce α-cellulose or sugar palm cellulose (SPC).

Isolation of sugar palm nanocrystalline cellulose

Acid hydrolysis of the obtained cellulose was conducted for the preparation of SPNCC. The operating conditions employed for this process include aqueous H_2SO_4 of 60 wt. % and mechanical stirring with a rotation speed of 1200 rpm at 45°C for a manipulated

variable period of 30, 45, and 60 min, denoted as SPNCC-I, SPNCC-II, and SPNCC-III, respectively. The obtained cellulose-to-liquor ratio was 5:100 (wt. %) (5 g cellulose:100 g H_2SO_4 solution). The centrifugation process (6000 rpm, 20 min, and 10°C) was then carried out to wash out leftover H_2SO_4 from the hydrolyzed cellulose samples. The suspensions were dialyzed against distilled water until a constant pH was reached (6.5–7) and the resultant suspension was sonicated for 30 min. Finally, the suspension was freeze-dried and then stored in a cool place prior to sample analysis.

Characterization

Chemical compositions. The chemical compositions of SPF, SPBF, and SPC fiber were determined according to the method described by Wise et al.[63] (holocellulose in wood and pulp) and TAPPI standard methods T 222 (acid-insoluble lignin in wood and pulp) and T 203 (alpha-, beta-, and gamma-cellulose in pulp).[39]

Field emission scanning electron microscopy. An FEI NOVA NanoSEM 230 machine (FEI, Brno-Černovice, Czech Republic) with 3 kV accelerating voltage aided the field emission scanning electron microscopy (FESEM) analysis. The entire samples were encapsulated in gold by a utilizing argon plasma metallizer (sputter coater K575X) (Edwards Limited, Crawley, UK) to avoid unwanted charging.

Transmission electron microscopy. A Philips Tecnai F20 transmission electron microscopy (TEM) machine with 200 kV accelerating voltage and a standard slanted sample holder was used to obtain nanostructure images of SPNCC.

Atomic force microscopy. Atomic force microscopy (AFM) analysis was performed by using a Dimension Edge with high-performance AFM tool (Bruker, Santa Barbara, CA, USA) assisted with Bruker Nanoscope Analysis software (Version 1.7) functioning using the Peak/Force Tapping mode with a single controller (Nanoscope V from Bruker) for the estimation of the thickness of SPCCs. A drop of SPNCC suspension was dropped on the surface of an optical glass slide and was set to air dry. Then, SPNFC samples were scanned at room temperature and controlled relative humidity in the tapping mode with OMCL-AC160TA standard Si probes (radius of tip of less than 10 nm, spring constant of 2.98 N m^{-1}, and resonant frequency of ~310 kHz) under a scan rate of 1 Hz.

Density. All fibers were dried for 7 days in a desiccator with phosphorus pentoxide (P_2O_5) as the drying agent

prior to density testing. The density of all fibers was determined using an AccuPyc 1340 pycnometer with gas intrusion under helium gas flow. The processes were carried out for five different specimens and their densities were calculated as an average value of the measurements.

Yield. The initial weight of SPC was used as the basis to calculate the nanocellulose yield obtained after hydrolysis treatment (30, 45, and 60 min). SPNCC suspensions obtained after dialysis were subject to the freeze-drying process. The yield was determined by using Equation (1), where M_i and M_f represent the initial and final weight of the samples before and after the freeze-drying process, respectively

$$\text{Yield}(\%) = \frac{M_f}{M_i} \times 100 \tag{1}$$

X-ray diffraction. A Rigaku D/max 2500 X-ray powder diffractometer (Rigaku, Tokyo, Japan) fixed with Cu-Kα radiation ($\lambda = 0.1541$ nm) in the 2θ range of 10–40° was used to investigate the X-ray diffraction (XRD) pattern of the fibers. The evaluation of the crystallinity index of the samples (X_c) was made possible by utilizing the empirical technique reported by Segal et al.,[64] as depicted in Equation (2). I_{002} and I_{am} are the peak intensities of crystalline and amorphous materials, respectively

$$X_c = \frac{I_{002} - I_{am}}{I_{002}} \times 100 \tag{2}$$

Zeta potential. The determination of the estimated size and the characterization of the surface charge properties of SPNCC were performed using a Zetasizer Nano-ZS (Malvern Instruments, Worcestershire, UK) by measuring the zeta potential of the fiber samples. Each fiber sample was diluted 10-fold in distilled water to 1 ml total volume and then placed into a particle size analyzer at room temperature (i.e., 25 ºC). Based on the Helmholtz–Smoluchowski equation, the analysis involved electrophoretic mobility (μm s^{-1}) of the nanofibers that was converted to zeta potential by inbuilt software.

Degree of polymerization. The degree of polymerization (DP) for each treated fiber suspension was measured based on the intrinsic viscosity. Measurement of viscosity was carried on according to TAPPI Standard Method T230 om-08 and ISO 5351-1, as reported by

Chauve et al.[65] The treated fibers were diluted in solutions containing distilled water and copper (II) ethylenediamine (CED) solution as a solvent with a ratio of 0.01:1:1 (treated fiber:distilled water:CED). The solution was shaken until all fibers were completely dissolved. The viscosity of the solvent and solution was measured at 25°C using an Ubbelohde viscometer tube (Type 231, PTA Laboratory Equipment, Vorchdorf, Austria) in triplicate for all samples. The molecular weight of the treated fiber was calculated using the Mark–Houwink approach, using the following equation

$$[\eta] = KM^{\alpha} \tag{3}$$

where $[\eta]$ the intrinsic viscosity and M is the molecular weight. The values of the constants were taken as $K = 0.42$ and $\alpha = 1$ for the CED solvent.[66]

Surface area and porosity measurements. The surface area, pore size, and pore size distribution were measured by the Brunauer–Emmett–Teller (BET) method or N_2 adsorption–desorption at 77 K by using surface area and porosity analyzer BELSorp Mini II (NIKKISO, Osaka, Japan). The samples were degassed at 105ºC under vacuum condition for 10 h. Specific surface areas were derived from the linear region of the isotherms using the BET equation in a relative P/Po pressure range of 10^{-2} to 1, whereas pore size distributions were calculated from the adsorption branch of the isotherms by the Barrett–Joyner–Halenda (BJH) method. The total pore volumes were estimated from the amount absorbed at a relative pressure of P/Po $= 0.98$.

Fourier transform infrared spectroscopy. A Fourier transform infrared (FTIR) spectrometer (Nicolet 6700 AEM, Thermo Nicolet Corporation, Madison WI, USA) was used to characterize the FTIR spectra of fibers within the wavenumber range of $4000-500$ cm^{-1} with a total of 42 scans at 4 cm^{-1} resolution.

Thermogravimetric analysis. The determination of the thermal stability of the samples was performed using a Q series thermal analysis machine from TA Instruments (New Castle, DE, USA). The operating conditions were temperature of 25–600°C, dynamic nitrogen environment, and 10°C min^{-1} heating rate. Samples of 5–15 mg were placed in an aluminum vessel prior to heating. The determination of weight loss was made possible by utilizing the thermogravimetric analysis (TGA) curve bearing a plot of percent weight loss versus temperature.

Table 1. Chemical composition of sugar palm fiber (SPF), sugar palm bleached fiber (SPBF), and sugar palm cellulose (SPC)

Fibers	Holocellulose (%)	Cellulose (%)	Hemicellulose (%)	Lignin (%)	Extractive (%)	Ash (%)
SPF	51.12	43.88	7.24	33.24	2.73	1.01
SPBF	76.47	56.67	19.8	0.27	0.23	2.16
SPC	86.3	82.33	3.97	0.06	–	0.72

Results and discussion

Chemical composition

The chemical compositions of the SPF, SPBF, and SPC are shown in Table 1. SPF consists of 43.88% cellulose and 33.24% lignin, which were increased by 12.79% and reduced by 32.97%, respectively, after treating the SPFs with $NaClO_2$ solution for cellulose and lignin, respectively. The utilization of $NaClO_2$ during the first stage of treatment was an excellent choice for lignin removal, as natural fiber can be considered as a composite of hollow cellulose fibrils reinforced by lignin as a binder in a hemicellulose matric.[67] This eased hemicellulose removal after that of lignin.[62] The significant reduction of the hemicellulose content in fiber occurred during NaOH treatment, which was 3.97% from 19.8%. Lignin and hemicellulose were solubilized by bleaching and dilute alkali treatment, respectively. This might be attributed to the cleavage of the ester-linked substance of hemicellulose, where this treatment increased the surface area of the SPF to make polysaccharides more vulnerable to hydrolysis.[62] Besides that, after the alkali treatment, the α-cellulose content was increased from 43.88% to 82.33%, whereas hemicellulose content was decreased from 7.24% to 3.97%. According to Alemdar and Sain,[68] the changes of chemical composition of the fiber after acid and alkaline treatments would results in a better degree of crystallinity of cellulose and, therefore, improve the strength and thermal properties of the fibers.[69,70]

Physical properties of fibers

The physical properties of SPF, SPBF, SPC, and SPNCC were determined using Image J software using images collected from TEM, FESEM, and AFM analysis. Figure 1(a) shows that for SPF with diameter size of $212.01 \pm 2.17\,\mu m$, the diameter decreased after the acid and alkali treatments. The diameters of SPBF and SPC were reduced to 121.80 ± 10.57 and $11.87 \pm 1.04\,\mu m$, respectively. This might be attributed to the partial removal of lignin and hemicelluloses; in other words, because of the elimination of the primary walls, which was further supported by the chemical analysis data given in Table 1. According to Rosa et al.[71] and Alemdar and Sain,[68] who worked with coconut fiber and wheat straw and soy hull, respectively, these images showed the partial removal of impurities pectin, lignin, and hemicellulose after chemical treatments, which acted as cementing components surrounding the fiber-bundles. Besides that, the surface of SPC (Figure 1(c)) had changed to smooth and groovy with parallel arrangement along the cellulose.

Several studies hypothesized a convergence between the effects of hydrolysis conditions on the physical properties. The studies revealed that the concentration of acid, ratio of acid to fiber, temperature, and time of hydrolysis process were crucial in defining the dimensions and morphology of the yielded NCC.[49,72] Figure 1 also shows the aqueous suspension (2 wt. %) for the TEM, FESEM, and AFM microscopies of SPNCC-I, SPNCC-II, and SPNCC-III. For the TEM nanoscopy image of SPNCC-I (Figure 1(d)), it can be observed that the SPNCC-I nanoscale structures were arranged and well-aligned with each other in bulky bundles. This might be ascribed to the diminutive reaction time in the partial depolymerization of SPC microfibrils.

SPNCC nanostructures produced from sugar palm-derived cellulose possessed a needle-shaped form, which is obviously displayed by SPNCC-II and SPNCC-III in Figures 1(h) and (f), respectively. From these figures, it can be perceived that both SPNCC-II and SPNCC-III had well- and uniformly distributed nanofiber morphology with good stability in colloidal suspension. The observed bundles of SPNCC that were arranged in parallel aligned for both SPNCCs were due to the hydrophilic copper grid substrate that stimulated the self-assembly process of nanoparticles through strong lateral hydrogen bonding.

Besides that, the diameter of SPNCC-I was approximately $13 \pm 1.73\,nm$, which presented an insignificant diameter difference, compared with those of SPNCC-II of approximately $9 \pm 1.96\,nm$ and SPNCC-III with an average value around $7.5 \pm 1.35\,nm$ (Table 2). The present discovery in TEM analysis is supported by the previous literature, with the estimated diameter size of NCC from kenaf (5.4–25.9 nm)[73] and jute (10–12 nm).[74]

The reduction of the SPNCC-I diameter compared to SPC was 99.89% based on Table 1, which was due to the removal of amorphous regions via hydrolysis
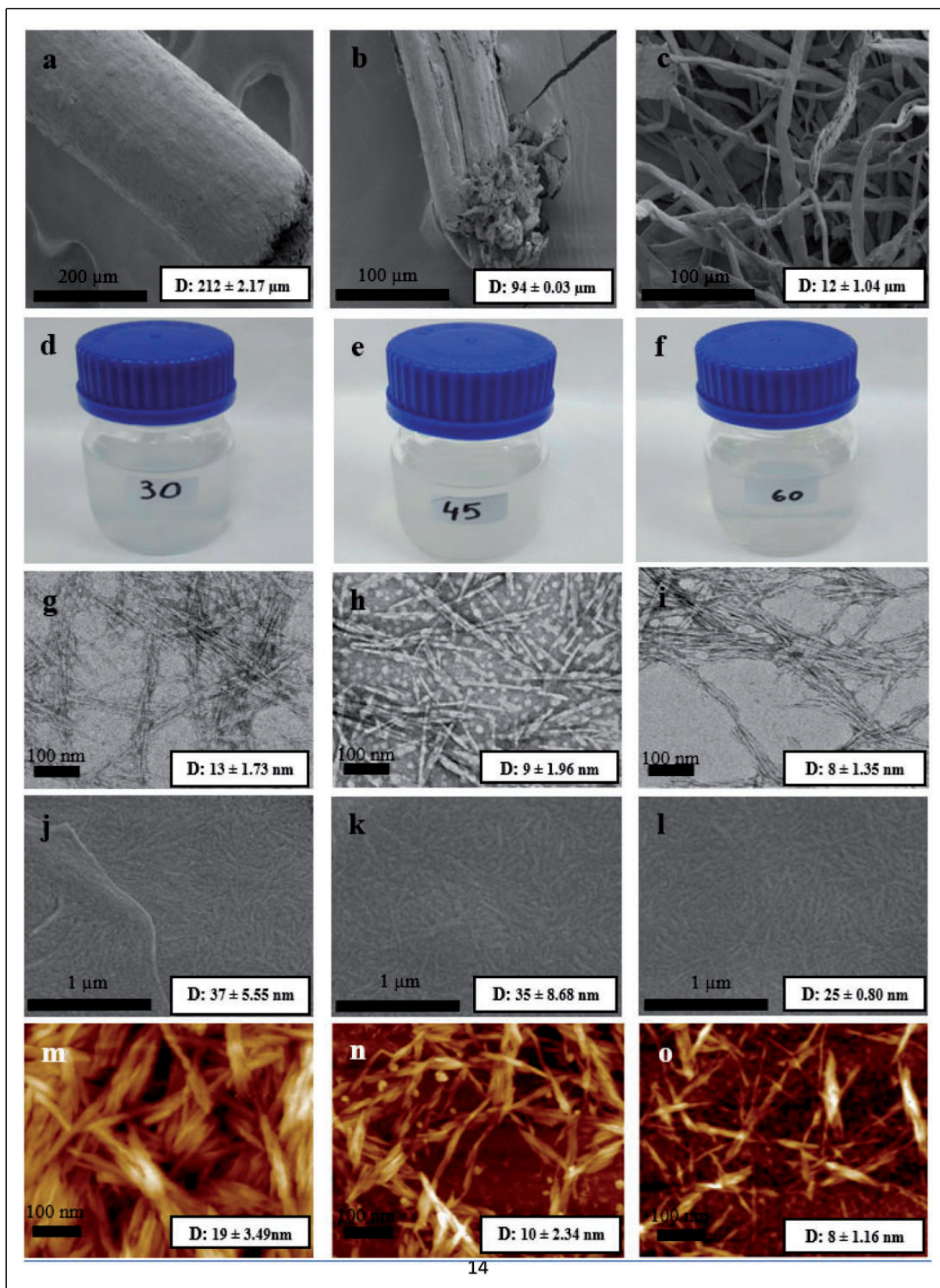
Figure 1. Field emission scanning electron microscopy (FESEM) micrographs of sugar palm fiber (a), sugar palm bleached fiber (b), sugar palm cellulose (c); aqueous suspension of (2 wt. %) (d), (e), (f); TEM images (g), (h), (i); FESEM images (j), (k), (l); AFM images (m), (n), (o). Images of SPNCC-I (d), (g), (j), (m), SPNCC-II (e), (h), (k), (n), and SPNCC-III (f), (i), (l), (o). SPNCC: sugar palm nanocrystalline cellulose; D: diameter.

Table 2. Physical properties of sugar palm fiber (SPF), sugar palm bleached fiber (SPBF), sugar palm cellulose (SPC), and sugar palm nanocrystalline cellulose (SPNCC)

Samples	Diameter	(Length) (nm)	Density (g/cm^{-3})	X_c (%)	Surface area (m^2/g)	Pore volume (cm^3/g)	DP	M_w (g/mol)
SPF	212 ± 2.17 μm	–	1.50	55.8	7.58	6.10 × 10^{-2}	–	–
SPBF	94 ± 0.03 μm	–	1.30	65.9	10.35	6.78 × 10^{-2}	2963.33	480,513.39
SPC	12 ± 1.04 μm	–	1.28	76.0	13.18	19.50 × 10^{-2}	946.48	153,458.51
SPNCC-I	13 ± 1.73 nm	175 ± 37.01	1.07	81.0	14.23	21.15 × 10^{-2}	226.19	36,677.53
SPNCC-II	9 ± 1.96 nm	130 ± 30.23	1.05	85.9	14.47	22.60 × 10^{-2}	142.86	23,164.74
SPNCC-III	8 ± 1.35 nm	105 ± 33.69	0.95	83.5	15.13	23.45 × 10^{-2}	107.14	17,373.56

Results expressed as mean ± standard deviation.
DP: degree of polymerization.

treatment on SPC. Hydrolysis process was continued for SPNCC-II and SPNCC-III for 45 and 60 min, respectively. This caused the size of SPNCC to reduce by 31% and 42% compared to SPNCC-I, respectively. This might be resulted by a longer reaction time of H_2SO_4 via hydrolysis treatment on fibers, which removed amorphous regions from nanofibers. Furthermore, a longer hydrolysis time could irritate the structure (length and diameter) of the SPNCC. Thus, a longer hydrolysis time led to shorter length and diameter of nanofibers. However, this depended on the conditions of the hydrolysis process and varieties of cellulosic fiber sources.[73]

The longest SPNCC was recorded for SPNCC-I, with the length of 175 ± 37.01 nm, and decreased slightly by 31%, to 130 ± 30.23 nm, for SPNCC-II. This trend of decrement throughout the extended hydrolysis time from 45 to 60 min was determined by observing the 42% decreasing length for SPNCC-III, with an average value of 105 ± 33.69 nm compared to SPNCC-I. Optimum aspect ratios (length to diameter) can be calculated by obtaining the values of length and diameter. Thus, from the calculation, the values of optimum aspect ratios for SPNCC-I, SPNCC-II, and SPNCC-III were 13.46, 14.44, and 13.13, respectively. These values were higher compared to the values from other NCCs originated from agro-residue sources, such as sago seed shells (5)[50]; however, the values were lower compared to pistachio shells (16).[54]

Furthermore, according to FESEM analysis, instead of a bulky bundle of structure displayed by SPNCC in TEM analysis, SPNCC-I (Figure 1(j)) had an individually long and fine nanofibrous structure. This phenomenon might be attributed to the freeze-drying process and high-intensity electron beam in the FESEM observation, which damaged the cellulose and pierced its structure, which was previously bundled into individual nanofibers. SPNCC-II (Figure 1(k)) and SPNCC-III (Figure 1(l)) demonstrated an asymmetrical rod-like shape instead of needle-like shape in TEM nanograph analysis. This was due to the tiny nanofiber fragments that tended to accumulate with individual SPNCC nanocrystals by interfacial hydrogen bonds.[75,76] Such accumulation was possible, as verified by FESEM analysis, that apparently showed a wider diameter size of SPNCC-II (9 ± 1.96 nm) compared to SPNCC-II (35.0 ± 8.68 nm) in TEM nanographs. In the analysis of AFM topographic nanograph images, SPNCC-I (Figure 1(m)) had a wide and long fibrous shape-form, which was consistent with the morphology of nanofibers obtained from TEM nanographs. SPNCC-II (Figure 1(n)) displayed denser crystallites compared to SPNCC-III (Figure 1(o)). Indeed, both SPNCC-II and SPNCC-III showed needle-like form, which was in good agreement with the TEM study. Furthermore, the calculated average values for SPNCC-I, SPNCC-II, and SPNCC-III from AFM analysis were higher compared to TEM nanograph analysis; however, the values obtained were within the diameter of FESEM. This phenomenon might be ascribed to the overestimation of nanoparticle dimensions by the tip broadening effect in AFM analysis. Based on the comparison of all results from the microscopy images taken by TEM, FESEM, and AFM equipment, it can be concluded that the clearest images of the resultant SPNCC morphology were the images from TEM analysis with the diameter size of 9 ± 1.96 nm. However, AFM microscopy is commonly performed for accurately measuring the height of nanofibers. The peak nanofiber heights of SPNCC-I, SPNCC-II, and SPNCC-III were 7.703, 5.781, and 4.655 nm, respectively.

Density, surface area, and porosity of fibers

One of the parameters that has to be considered in the process of material selection is weight, as it influences the performance of the products. In correlation to that, density is the key criterion that is interrelated with these

fiber weight properties. The density value of SPF, SPBF, SPC, SPNCC-I, SPNCC-II, and SPNCC-III showed a decreasing pattern throughout the treatments, which were 1.50, 1.30, 1.28, 1.07, 1.05, and 0.95 g/cm^{-3}, respectively. This trend might be attributed to the removal of the main component of the fibers, such as lignin and hemicellulose, as displayed in Table 1. The removal of amorphous non-cellulosic compound components, such as lignin and hemicellulose, in bleaching and alkali treatment created voids in the structure of fibers that would lead to fiber swelling. The component of the fibers then became well separated, which increment in volume with loss in weight caused the density to decrease.[77]

Besides that, from Table 1, it can be observed that the densities of SPNCC-I, SPNCC-II, and SPNCC-III decreased insignificantly throughout the prolongation of the hydrolysis process, with the values of 1.07, 1.05, and 0.95, respectively. This trend was the result of the removal of amorphous regions that were attached to crystalline regions that occurred due to the extended hydrolysis treatment producing abysses or spaces in the nanofiber structure. This swelled and separated the nanofibers into individual crystallites. According to Ray and Sarkar,[77] the increment in the volume of fiber and loss in weight would affect the reduction in the density values. Moreover, the SPNCC densities of all treatments were lower compared to conventional fibers, such as glass fiber (2.5 g/cm^3), aramid (1.4 g/cm^3), and carbon (1.7 g/cm^3).[78]

The density of fiber is related to the surface area and the porosity of fibers. The higher the pore volume, the lower the density of the fiber. It can be observed that the cumulative pore volumes of SPF, SPBF, SPC, SPNCC-I, SPNCC-II, and SPNCC-III increased throughout the treatments, with values of 6.10×10^{-2}, 6.78×10^{-2}, 19.50×10^{-2}, 21.15×10^{-2}, 22.60×10^{-2}, and 23.45×10^{-2} (cm^3/g), respectively. The cumulative pore volume for SPNCC-II (22.60×10^{-2} cm^3/g) is four times larger than for SPF (0.061 cm^3/g). This was due to the closely aligned, rigid, and tightly bounded building elements via strongly hydrogen bonded cellulose structures, hence leaving few interfacial spaces.[79] The result of low pore volume was supported by the FESEM, and AFM (Figure 1). The pore volumes of SPNCC-I, SPNCC-II, and SPNCC-III were observed to increase after the loosely packed structures took shape to create a huge amount of mesopores among the SPNCC. A similar trend was observed with the BET surface area for SPF, SPBF, SPC, SPNCC-I, SPNCC-II, and SPNCC-III, which were 7.58, 10.35, 13.18, 14.23, 14.47, and 15.13 m^2/g, respectively. The BET surface area of SPNCC-II was two times larger compared to SPF. The higher specific surface area

of the nanofibers assembled from SPNCC might be attributed to the smaller fiber sizes compared with those of SPF.

Degree of polymerization

The DP is an important parameter for determining the length and branching of cellulose chains. Besides that, it also functions to evaluate the effect of hydrolysis in the cellulose chains that are present in nanocellulose. Frenot et al.[80] stated that the DP and molecular weight (M_w) might affect the properties of cellulose, such as solubility and spinnability, as well as the mechanical properties of cellulose-based materials. The DP and viscosity-average M_w of the treated fibers were determined using an intrinsic viscosity measurement. Table 1 displays the DP values for the various treated fibers prepared in this study. The DP of the SPBF, SPC, SPNCC-I, SPNCC-II, and SPNCC-III were 2963.33, 946.48, 226.19, 142.86, and 107.14, respectively, and the molecular weights were 480,513.39, 153,458.51, 36,677.53, 23,164.74, and 17,373.56 g/mol, respectively. It is observable that the DP obtained for the SPC was almost similar to the DP of oil palm cellulose (967),[66] curaua cellulose (989),[81] and bamboo cellulose (891).[82]

Yasim-Anuar et al.[66] reported that the DP and M_w of cellulose-based material ranged from 400 to 3000 and 90,000 to 300,000 g/mol, respectively. The DP and M_w of SPF were in the range of the cellulose DP and M_w, and therefore they were in good agreement with those reported in the literature.[66]

The decreasing trend observed for the DP and M_w of SPBF, SPC SPNCC-I, SPNCC-II, and SPNCC-III might be due to the removal of lignin, hemicellulose, and the amorphous region via the acid, alkali, and hydrolysis treatments of the raw SPF. Through these treatments, SPF, SPBF, and SPC fibers were cleaved, releasing the NCC.[83] Besides that, according to Hubbell and Ragauskas,[84] the reduction of cellulose DP was due to the acid-catalyzed cleavage during acid-chlorite treatment. In addition, alkali treatment stimulated more reactive sites on the surface of cellulose.[81] This phenomenon might increase the effectiveness of the acid hydrolysis treatment that resulted in a major level of breaking the cellulose chains. Corrêa et al.[81] and Pääkkö et al.[85] reported that the sulfate group of strong acid led to an extensive hydrolysis of the amorphous phase and catalyzed the degradation of the cellulose chain, later reducing the DP. Thus, the longer the hydrolysis time, the smaller the DP value due to the degradation of amorphous regions and crystalline parts. The DP attained for SPNCC-II and SPNCC-II was similar to the DP of curaua nanofiber (101.6)[81] and sugar beet pulp (120).[86]

Table 3. Yield and zeta potential of SPNCC-I, SPNCC-II, and SPNCC-III

Fibers	Yield (%)	Z-average (nm)	Zeta-potential (mV)	Conductivity (mS/cm)
SPNCC-I	33.51%	192.62 ± 22.56	−20.66 ± 5.25	0.036 ± 0.001
SPNCC-II	29.01%	138.93 ± 13.91	−61.50 ± 1.65	0.051 ± 0.001
SPNCC-III	13.12%	76.94 ± 2.20	−63.54 ± 1.59	0.101 ± 0.002

SPNCC: sugar palm nanocrystalline cellulose.

SPNCC yield and zeta potential

The isolated SPNCC yields of SPF from various treatments according to specific times of 30, 45, and 60 min are summarized in Table 3. The highest yield was recorded for SPNCC-I with 33.5% and decreased to 29.01% for SPNCC-II. The decreasing trend throughout the hydrolysis extended time from 45 to 60 min can be observed in the SPNCC-III and SPNCC-II decreasing yields of 15.89% and 13.12%, respectively. The low yield of SPNCC might resulted from the gradual disintegration of amorphous regions and the degradation of crystalline parts during extended hydrolysis time. The attained SPNCC yield in this work was in agreement with the nanocrystals from mengkuang leaves (28%) and sisal yield (30%) reported by Sheltami et al.[40] and Garcia de Rodriguez et al.,[45] respectively. However, de Morais Teixeira et al.[87] addressed that the yield of NCC from sugarcane bagasse agro-residue was 58%, which almost doubled the yield of SPNCC. The dissimilarities of the obtained NCC yield were influenced by the difference in the sources and origins of the used fibers, fiber pretreatment, and hydrolysis process conditions (i.e., type and concentration of acid used, temperature, and time).[88]

Zeta potential

Table 3 also presents the zeta potential and conductivity values of SPNCC-I, SPNCC-II, and SPNCC-III. The nanocellulose suspension stability was based on the measurement of zeta potential. The incorporation of sulfate groups embedded on NCC caused the existence of negatively charged nanomaterials. This phenomenon was due to the hydrolysis of sulfuric acid, which promoted the formation of negative electrostatic layers for covering and encapsulating nanocellulose, and hence stimulated their dispersion in water.[50] High surface charging modifications of SPNCC-I, SPNCC-II, and SPNCC-III with the values of −20.66 ± 5.25, −61.50 ± 1.65, and −63.54 ± 1.59 mV, respectively, were due to the great incorporation of sulfate groups into SPNCC during sulfuric acid hydrolysis.[89] From Table 3, all SPNCC nanofibers demonstrated zeta potential values larger than −15 mV, which indicated
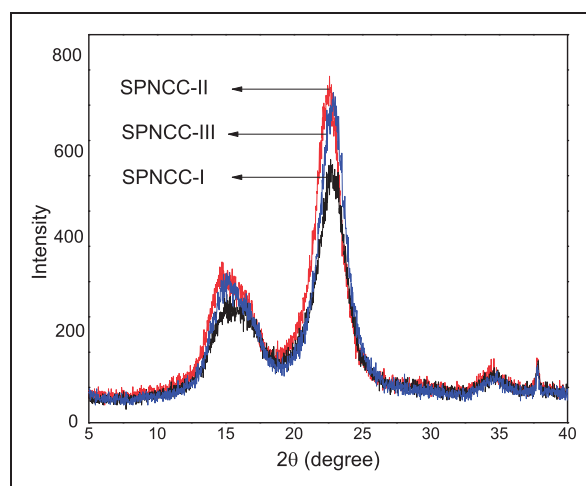

Figure 2. X-ray diffraction patterns of SPNCC-I, SPNCC-II, and SPNCC-III. SPNCC: sugar palm nanocrystalline cellulose.

that SPNCC possessed good stability of dispersion in an aqueous suspension.[89] These large negatively charged zeta potential values were due the properties of cellulose fibers that possessed –OH functional groups and produced negatively charged polymers. The suspension of Nanofibrillated cellulose (NFCs) was considered to be stable as the absolute values were lower than -30mV and higher than 30 mV.[50] According to Naduparambath et al.,[50] nanofibers will exist in the agglomeration form if the value of zeta potential is between −15 and 15 mV. This is because, within this value, the nanofibers did not have sufficient charge to repulse each other, thus forming agglomeration. Moreover, small zeta potential values showed weak electrostatic repulsive force among Sugar palm nanofibrillated cellulose (SPNCC).[50] The value of conductivity also increased as the value of zeta potential increased. According to Kian et al.,[89] the electrostatic repulsive forces between nanofibers became stronger when more sulfate groups were attached to the surface of the nanofibers, which then promoted higher negative zeta values of SPNCC-II compared to SPNCC-I. Furthermore, this phenomenon was also similar for SPNCC-III, as the hydrolysis time continued until 60 min, which resulted in significantly larger values of zeta potential than those of SPNCC-II. This might be

due to the SPNCC-III geometry with much smaller diameter values compared to SPNCC-I and SPNCC-II, thus displaying an increased surface area sulfated by sulfuric acid.[90]

X-ray diffraction measurements

The changes in crystallinity profile of the fibers at all stages of treatment were analyzed using XRD analysis. The degree of crystallinity were calculated by using the Segal formula and is summarized in Table 2. The crystallinity indices of SPF, SPBF, SPC, SPNCC-I, SPNCC-II, and SPNCC-III were found to increase significantly: 55.8%, 65.9%, 76.0%, 81.0%, 85.9%, and 83.5%, respectively. The higher crystallinity value of SPNCCs compared to sugar palm fibers can be well understood by the removal of amorphous non-cellulosic compounds, such as lignin and hemicellulose, induced by the acid, alkali, and hydrolysis treatments that took place during the purification process. To be more focused on the effect of hydrolysis time on the crystallinity of SPNCC, Figure 2 shows the crystallinity patterns of SPNCC-I, SPNCC-II, and SPNCC-III. The characterization data of nanofiber polymorphs obtained from XRD diffractograms showed that the presence of cellulose type I (-110 and 200) was observed at the peaks of $2\theta = 15°$ and 22.6°, respectively, and cellulose II was detected at the peaks of $2\theta = 12.3°$ and 22.1°.[91] X-ray diffractogram patterns from Figure 2 displayed a major intensity peak at $2\theta = 22.6°$ for all nanofiber samples, which indicated a crystalline structure of cellulose type I, whereas a low amorphous region was detected at the low intensity peak of $2\theta = 18°$.[64] The major intensity peaks for SPNCC-I, SPNCC-II, and SPNCC-III nanofibers were observed at 22.68°, 22.88°, and 22.6°, respectively, and the minor intensity peaks at 18.72°, 19.28°, and 19.06°, respectively. The resulting XRD profiles indicated a mixture of polymorphs of cellulose type I (typical peaks at $2\theta = 15°$ and 22.6°).[91] From Table 2, the highest crystallinity index of 85.90% was observed for SPNCC-II with its narrow peak at 22.88°. However, SPNCC-III exhibited a slightly decreased diffraction peak at 22.88° with a crystallinity degree of 83.50% compared to SPNCC-II. This phenomenon occurred possibly due to severe hydrolysis conditions that resulted in the reorientation of the crystalline lattice order in (200).[92] The extended hydrolysis reaction suggested that the extraction time of 60 min was severe enough, as this duration removed the amorphous regions of nanofibers and also partly disintegrated the crystalline regions. SPNCC-I showed the poorest crystallinity index value of 80.97% with intense peaks at 15° and 22.68°, where the peak at 15.0° corresponded to the (110) plane presence of amorphous regions. Furthermore, it has been
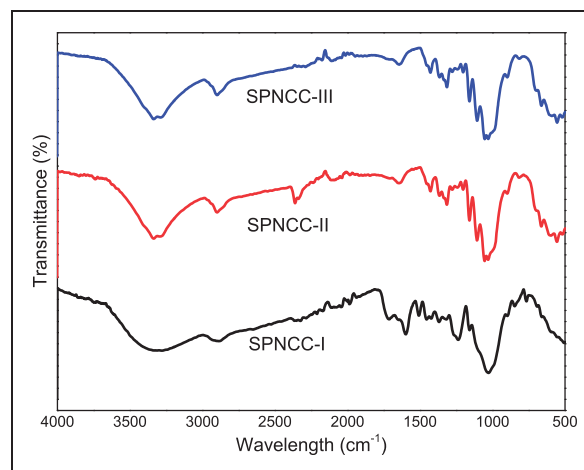

Figure 3. Fourier transform infrared spectra of SPNCC-I, SPNCC-II, and SPNCC-III. SPNCC: sugar palm nanocrystalline cellulose.

proven that the removal of amorphous regions that were more degradable by hydronium ions tended to produce high-crystallinity SPNCC crystallites, signifying that the extended hydrolysis reaction was effective.[92] The crystallinity degree of fibers was increased with the sharpness of diffraction peaks.[27,39,56,62] Even though the structure of the nanofiber crystals was not altered, the crystallinity index varied significantly among the nanofibers. The crystallinity indexes of SPNCC-I, SPNCC-II, and SPNCC-III were 80.97%, 85.90%, and 83.50%, respectively. These outcomes revealed that the material crystallinity was gradually increased with the extended hydrolysis time. The crystallinity index values of the respective nanofibers were higher compared to other agro-residual nanofibers, such as wheat straw (77.8%)[68] and pineapple leaves (54%).[93] Nevertheless, the values were still lower than NCC from agro-residue rice straw (91.2%).[79] The crystallinity indexes of nanofibers were directly interrelated to cellulose rigidity and nanofiber tensile strength. As the number of the crystalline index increased, the rigidity of cellulose increased and, thus, the tensile strength also increased. Therefore, these nanofibers could be used as reinforcement nanofiller in the nanocomposite field, as it would improve the mechanical properties of nanocomposites.

FTIR spectroscopy for physic-chemical analysis

Figure 3 displays the physic-chemical analysis of the FTIR spectral features of SPNCC-I, SPNCC-II, and SPNCC-III. With the increase of hydrolysis time, a wide band at 3200–3500 cm^{-1} that indicated the presence of O-H covalent bonds stretching with strong
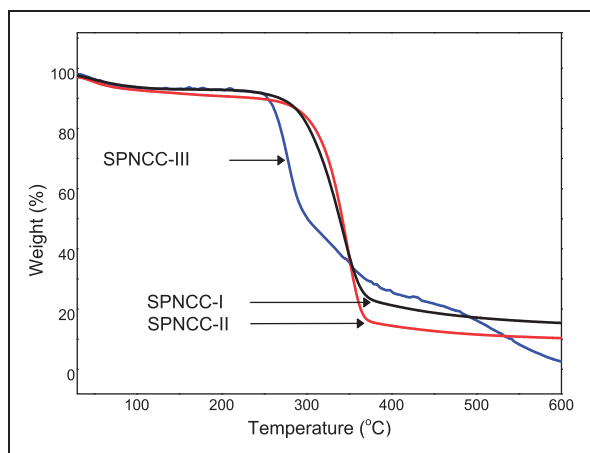
Figure 4. Thermogravimetry curves for SPNCC-I, SPNCC-II, and SPNCC-III. SPNCC: sugar palm nanocrystalline cellulose.
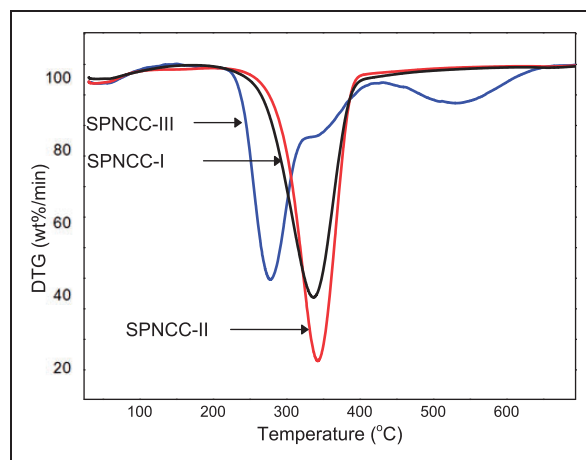
Figure 5. Derivative thermogravimetric curves for SPNCC-I, SPNCC-II, and SPNCC-III. SPNCC: sugar palm nanocrystalline cellulose.

intramolecular and intermolecular H-bonding became deeper. This occurred due to the presence of hydroxyl groups in nanofibers, which also signified the hydrophilic property of SPNCC.[94] A typical cellulose structure was observed at the peak of $897 \, cm^{-1}$, in which this spectrum displayed a slight increase in the absorbance band, around 1080 and $890 \, cm^{-1}$. This might due to the interaction between β-glycosidic linkages and the glucose units of cellulose, which also signified the removal of amorphous regions. Another wide region at $1160 \, cm^{-1}$ assigned to C-O-C asymmetric valence vibration became narrower and piercing due to the higher revelation of cellulose content.[95] Furthermore, the prominent peaks at $897 \, cm^{-1}$ (C-H rocking vibration), $1110 \, cm^{-1}$ (C-OH stretching), and $2900 \, cm^{-1}$ (C-H symmetrical stretching) linked to the presence of α-cellulose and NCC characteristics were more observable after extended hydrolysis treatment.[94,95] The indistinct change of intensity crests at $1370 \, cm^{-1}$ (C-H_2 deformation vibration) and $1316 \, cm^{-1}$ (C-H_2 rocking vibration) were observed between SPNCC-II and SPNCC-III, which might be attributed to the development or reorientation of the hydrogen bonding network in the crystal lattice of the NCC chemical structure and resulted in the reduction of CH_2 rocking vibration.[92] The sulfation peak of nanocellulose at $807 \, cm^{-1}$ indicated C-O-S bending vibration in C-O-SO^{3-} groups, and was detected in SPNCC-II and SPNCC-III spectra but observed to be insignificant in SPNCC-I spectra. This might be due to the extended hydrolysis time, where sulfuric acid had longer contact time with the nanofibers, and thus resided in NCC. The peak within the FTIR spectra of $1637 \, cm^{-1}$ (H-O-H stretching vibration), which was also related to common water absorption, showed an increasing intensity from SPNCC-I to SPNCC-III.[92]

Thermogravimetric analysis

Figure 4 shows TGA curves of SPNCC samples. Most of the SPNCC underwent the first stage of weight loss at the temperature range of 40–150°C. This is associated with the evaporation of moisture residue within the components of nanocellulose. In addition, all SPNCCs showed continued thermal degradation at the temperature range of 160–350°C, which is mainly linked to the degradation of the cellulosic chain.[96] SPNCC-III nanofibers displayed the lowest onset degradation with $T_{Onset} = 160.76°C$. This might contribute to the difference in organization of crystal structures, which is the reorientation and rearrangement of the crystalline structure in cellulose that occurred during the extended hydrolysis treatment. Besides that, the effect of the sulfate group on the surface of nanofibers also promoted the increase in the onset temperature of degradation. However, for SPNCC-I and SPNCC-II, T_{Onset} was located around 190.19°C and 185.78°C, respectively, which was possibly due to the well-aligned and rearrangement of crystalline structure of SPNCC-I and SPNCC-II that affected the thermal resistance of nanofibers toward initial temperature decomposition.[89] Starting from the initial thermal decomposition onwards, both SPNCC-I and SPNCC-II shifted their higher thermal decomposition temperatures toward higher temperature, until 335.15°C and 348.65°C, respectively, when compared with SPNCC-III (278.50°C). SPNCC-II showed the most stable curve and highest thermal stability from 185.78°C to 348.65°C that might be attributed to the unaffected and strong native crystal order in its crystalline structure.

In DTG analysis (Figure 5), the asymmetric curves of SPNCC-III with additional medium shoulders or humps in close proximity indicated multiple decompositions of the nanocellulose chain around 160–600°C. A defected TGA curve for SPNCC-III was possibly due to the sample being thermally unstable as a result of the greater heterogeneity of exposure of different contents, largely the sulfate group, incorporated on the surface area of the nanocellulose, which is then susceptible to heat degradation.[75,97] Nanocellulose with a high sulfated region tended to degrade at lower temperatures compared to less accessed sulfated regions, which were more thermally stable. The first6 thermal degradation observed at approximately 278.50°C was associated with the degradation of more sulfated regions or less thermally stable sulfonated nanocellulose, whereas a small hump (second thermal degradation) at 340.09°C was ascribed to the degradation of non-chemically modified cellulose regions or less accessed regions by sulfate groups of the acid. This phenomenon was supported by the research conducted by Mandal and Chakrabarty,[98] in which the first thermal degradation of SPNCC-III ($T_{Max} = 278.50$°C) and wide-range decomposition of SPNCC-III can be possibly assigned to the severe reduction in molecular weight and decomposition of more accessible parts in nanocellulose, which was contacted with highly sulfate amorphous regions. Beyond 420°C, the presence of the third degradation peak at 531.22°C was likely associated with the thermal resistance of the sulfur component that inhibited the decomposition of carbonaceous residues into low molecular weight components.

Both SPNCC-I and SPNCC-II presented insignificant differences of decomposition peak temperatures, which might be due to their relatively low effect of sulfur contact and crystallinity degree. Besides that, the decomposition peak temperature of SPNCC-III was lower than those of SPNCC-I and SPNCC-II, which was described earlier from the deposition of a large amount of sulfur that stimulated earlier nanocellulose decomposition.[94,99,100] High weight loss in the samples resulted in low residue formation at the end of the analysis. Herein, the TGA results revealed that the highest weight loss occurred in the sample of SPNCC-III, hence having the lowest amount of residue due to the combination effect of high crystalline fraction and large sulfate content contacted on the surface of nanocellulose.[94] SPNCC-II produced 17.97% residue, which was lower compared to SPNCC-I with the residue value of 19.5%. This revealed that SPNCC-II consisted of a higher composition of sulfate content being incorporated within nanocellulose. This was due to the comparatively low molecular weight of sulfate content compared with that of crystal lattice content.[94]

Conclusions

The duration of the hydrolysis process is a crucial single factor in obtaining a suspension of negatively charged isolated NCC in water suspension. The low yield of SPNCC can be explained by the disintegration of amorphous regions and extended degradation of crystalline regions. The findings in this current work presented an isolation of SPNCC from SPC using a moderately low chemical concentration of 60 wt. % H_2SO_4 solution, which gained a yield of 33.51%. Thus, this certified that hydrolysis process is a cost-saving isolation process. From the image morphology captured by TEM and AFM, all SPNCCs showed needle-shaped nanofibers; however, FESEM micro-images showed rod-shaped nanofibers. In the TEM analysis, SPNCC-II (45 min hydrolysis) showed the highest aspect ratio of 14.44, which suggested that SPNCC-II attained a high proficiency of mechanical improvement in the polymer nanocomposite field. Furthermore, in view of the dispersion stability, SPNCC-II displayed a well-dispersed characteristic in colloidal suspension, feasibly providing it with better nanocellulose distribution during the fabrication of nanocomposites. The XRD showed enrichment in the proportion of crystalline cellulose in nanocellulose. The crystallinity of the SPNCC-II was 30% higher than that of the raw fiber. Besides that, in terms of thermal properties, the SPNCC-II sample showed good stability compared to SPNCC-III due to the reinforcement of the sulfate constituent during sulfuric acid hydrolysis treatment. Therefore, it can be summarized from these results that SPNCC isolated from this current experiment can be used as a potential reinforcement nanomaterial in the future for the improvement of starch-based nanocomposites in the fields of food packaging, automotive, and biomedical applications.

ORCID iD

Mohd Sapuan Salit https://orcid.org/0000-0001-6622-2632

References

1. Ilyas RA, Sapuan SM, Sanyang ML, et al. Nanocrystalline cellulose as reinforcement for polymeric matrix nanocomposites and its potential applications: a review. *Curr Anal Chem* 2018; 14: 203–225.

2. Ilyas RA, Sapuan SM, Norizan MN, et al. Potential of natural fibre composites for transport industry: a review. In: *Prosiding seminar Enau Kebangsaan 2019*, Bahau, Negeri Sembilan, 1 April 2019, Paper no 1 : Institute of Tropical Forest and Forest Products (INTROP), Universiti Putra, Malaysia, 2019, pp.2–11.

3. Al-Oqla F and Sapuan MS. *Materials selection for natural fiber composites*. 1st ed. Duxford, UK: Elsevier Woodhead Publishing, 2017.

4. Ilyas RA, Sapuan SM, Ishak MR, et al. Development and characterization of sugar palm nanocrystalline cellulose reinforced sugar palm starch bionanocomposites. *Carbohydr Polym* 2018; 202: 186–202.

5. Aisyah HA, Paridah MT, Sapuan SM, et al. Thermal properties of woven kenaf/carbon fibre-reinforced epoxy hybrid composite panels. *Int J Polym Sci* 2019; 2019: 1–8.

6. Hazrol MD, Sapuan SM, Ilyas RA, et al. Electrical properties of sugar palm nanocrystalline cellulose, reinforced sugar palm starch nanocomposites. *Polimery* 2020; 55: 33–40.

7. Sapuan SM and Ilyas RA. Sugar palm: fibers, biopolymers and biocomposites. *INTROPica* 2017; 15: 5–7.

8. Sapuan SM, Ishak MR, Leman Z, et al. Development of products from sugar palm trees (Arenga Pinnata Wurb. Merr): a community project. *INTROPica* 2017; 13: 12–13.

9. Sanyang ML, Sapuan SM, Jawaid M, et al. Development and characterization of sugar palm starch and poly(lactic acid) bilayer films. *Carbohydr Polym* 2016; 146: 36–45.

10. Abral H, Basri A, Muhammad F, et al. A simple method for improving the properties of the sago starch films prepared by using ultrasonication treatment. *Food Hydrocolloid* 2019; 93: 276–283.

11. Ilyas RA, Sapuan SM, Ishak MR, et al. Water transport properties of bio-nanocomposites reinforced by sugar palm (Arenga Pinnata) nanofibrillated cellulose. *J Adv Res Fluid Mech Therm Sci J* 2018; 51: 234–246.

12. Sanyang ML, Ilyas RA, Sapuan SM, et al. Sugar palm starch-based composites for packaging applications. In: Jawaid M and Swain SK (eds) *Bionanocomposites for packaging applications*. Cham: Springer International Publishing, pp.125–147.

13. Ilyas RA, Sapuan SM, Ishak MR, et al. Sugar palm nanocrystalline cellulose reinforced sugar palm starch composite: degradation and water-barrier properties. In: *IOP Conference Series: Materials Science and Engineering, Volume 368, The Wood and Biofiber International Conference (WOBIC 2017)*, Selangor, Malaysia, 21–23 November 2017, 368, p. 012006 print 2018. DOI: 10.1088/1757- 899X/368/1/012006.

14. Ilyas RA, Sapuan SM, Ishak MR, et al. Nanocellulose reinforced starch polymer composites: a review of preparation, properties and application. In: *proceedings of the 5th international conference on applied sciences and engineering (ICASEA, 2018)*, 7-8 April 2018, pp.325–341. Cameron Highlands, Malaysia: Global Academic Excellence (M) SDN BHD.

15. Jumaidin R, Saidi ZAS, Ilyas RA, et al. Characteristics of cogon grass fibre reinforced thermoplastic cassava starch biocomposite: water absorption and physical properties. *J Adv Res Fluid Mech Therm Sci* 2019; 62: 43–52.

16. Jumaidin R, Khiruddin MAA, Asyul Sutan Saidi Z, et al. Effect of cogon grass fibre on the thermal, mechanical and biodegradation properties of thermoplastic cassava starch biocomposite. *Int J Biol Macromol* 2020; 146: 746-755.

17. Jumaidin R, Ilyas RA, Saiful M, et al. Water transport and physical properties of sugarcane bagasse fibre reinforced thermoplastic potato starch biocomposite. *J Adv Res Fluid Mech Therm Sci* 2019; 61: 273–281.

18. Islam MT, Alam MM and Zoccola M. Review on modification of nanocellulose for application in composites. *Int J Innovat Res Sci Eng Technol* 2013; 2: 5444–5451.

19. Nurazzi NM, Khalina A, Sapuan SM, et al. Mechanical properties of sugar palm yarn / woven glass fiber reinforced unsaturated polyester composites: effect of fiber loadings and alkaline treatment. *Polimery* 2019; 64: 12–22.

20. Halimatul MJ, Sapuan SM, Jawaid M, et al. Water absorption and water solubility properties of sago starch biopolymer composite films filled with sugar palm particles. *Polimery* 2019; 64: 27–35.

21. Halimatul MJ, Sapuan SM, Jawaid M, et al. Effect of sago starch and plasticizer content on the properties of thermoplastic films: Mechanical testing and cyclic soaking-drying. *Polimery* 2019; 64: 32–41.

22. Atiqah A, Jawaid M, Sapuan SM, et al. Physical and thermal properties of treated sugar palm/glass fibre reinforced thermoplastic polyurethane hybrid composites. *J Mater Res Technol* 2019; 8: 3726–3732.

23. Asyraf MRM, Ishak MR, Sapuan SM, et al. Woods and composites cantilever beam: a comprehensive review of experimental and numerical creep methodologies. *J Mater Res Technol* 2020; 9: 6759-6776.

24. Asim M, Abdan K, Jawaid M, et al. A review on pineapple leaves fibre and its composites. *Int J Polym Sci* 2015; 2015: 1–16.

25. Abral H, Atmajaya A, Mahardika M, et al. Effect of ultrasonication duration of polyvinyl alcohol (PVA) gel on characterizations of PVA film. *J Mater Res Technol* 2020; 9: 2477–2486.

26. Ilyas RA, Sapuan SM, Ishak MR, et al. Characterization of sugar palm nanocellulose and its potential for reinforcement with a starch-based composite. In: Sapaun SM, Ishak MR, Sanyang ML and Sahari J (eds) *Sugar palm biofibers, biopolymers, and*

biocomposites. 1st ed. Boca Raton, FL: CRC Press/ Taylor & Francis Group, CRC Press, 2018, pp.189–220.

27. Ilyas RA, Sapuan SM, Ishak MR, et al. Sugar palm nanofibrillated cellulose (Arenga pinnata (Wurmb.) Merr): effect of cycles on their yield, physic-chemical, morphological and thermal behavior. *Int J Biol Macromol* 2019; 123: 379–388.

28. Sapuan SM, Ilyas RA, Ishak MR, et al. Development of sugar palm–based products: a community project. In: Sapaun SM, Ishak MR, Muhammad Lamin Sanyang and Sahari J (eds) *Sugar palm biofibers, biopolymers, and biocomposites*. 1st ed. Boca Raton, Florida: CRC Press/ Taylor & Francis Group, CRC Press, 2018, pp.189–220.

29. AL-Oqla FM and El-Shekeil YA. Investigating and predicting the performance deteriorations and trends of polyurethane bio-composites for more realistic sustainable design possibilities. *J Clean Prod* 2019; 222: 865–870.

30. AL-Oqla FM and Sapuan SM. Investigating the inherent characteristic/performance deterioration interactions of natural fibers in bio-composites for better utilization of resources. *J Polym Environ* 2018; 26: 1290–1296.

31. AL-Oqla FM and Sapuan SM. Polymer selection approach for commonly and uncommonly used natural fibers under uncertainty environments. *JOM* 2015; 67: 2450–2463.

32. Bledzki AK and Gassan J. Composites reinforced with cellulose based fibers. *Prog Polym Sci* 1999; 24: 221–274.

33. Syafri E, Sudirman, Mashadi, et al. Effect of sonication time on the thermal stability, moisture absorption, and biodegradation of water hyacinth (Eichhornia crassipes) nanocellulose-filled bengkuang (Pachyrhizus erosus) starch biocomposites. *J Mater Res Technol* 2019; 8: 6223–6231.

34. Ilyas RA and Sapuan SM. The preparation methods and processing of natural fibre bio-polymer composites. *Curr Org Synth* 2020; 16: 1068–1070.

35. Mazani N, Sapuan SM, Sanyang ML, et al. design and fabrication of a shoe shelf from kenaf fiber reinforced unsaturated polyester composites. In: Ariffin H, Sapuan SM and Mohd Ali Hassan (eds) *Lignocellulose for future bioeconomy*. Oxford, United Kingdom, Elsevier, 2019, pp.315–332.

36. Abral H, Ariksa J, Mahardika M, et al. Highly transparent and antimicrobial PVA based bionanocomposites reinforced by ginger nanofiber. *Polym Test* 2019; 81: 106186.

37. Jacob M and Thomas S. Biofibers and biocomposites. *Carbohydr Polym* 2008; 71: 343–364.

38. Kathirselvam M, Kumaravel A, Arthanarieswaran VP, et al. Isolation and characterization of cellulose fibers from Thespesia populnea barks: a study on physicochemical and structural properties. *Int J Biol Macromol* 2019; 129: 396–406.

39. Ilyas RA, Sapuan SM and Ishak MR. Isolation and characterization of nanocrystalline cellulose from sugar palm fibres (Arenga Pinnata). *Carbohydr Polym* 2018; 181: 1038–1051.

40. Sheltami RM, Abdullah I, Ahmad I, et al. Extraction of cellulose nanocrystals from mengkuang leaves (Pandanus tectorius). *Carbohydr Polym* 2012; 88: 772–779.

41. Asrofi M, Abral H, Putra YK, et al. Effect of duration of sonication during gelatinization on properties of tapioca starch water hyacinth fiber biocomposite. *Int J Biol Macromol* 2018; 108: 167–176.

42. Asrofi M, Abral H, Kasim A, et al. Isolation of nanocellulose from Water Hyacinth Fiber (WHF) produced via digester-sonication and its characterization. *Fiber Polym* 2018; 19: 1618–1625.

43. Abral H, Dalimunthe MH, Hartono J, et al. Characterization of tapioca starch biopolymer composites reinforced with micro scale water hyacinth fibers. *Starch/Staerke* 2018; 70: 1–8.

44. Ilyas RA, Sapuan SM, Ishak MR, et al. Water barrier properties of biodegradable films reinforced with nanocellulose for food packaging application: a review. In: Sapuan SM, Noor Azammi AM, Ilyas RA (eds) 6*th postgraduate seminar on natural fiber reinforced polymer composites 2018*, Institute of Tropical Forestry and Forest Products (INTROP), Universiti Putra Malaysia, Serdang, Selangor, 4 December 2018, pp.55–59.

45. Garcia de Rodriguez NL, Thielemans W and Dufresne A. Sisal cellulose whiskers reinforced polyvinyl acetate nanocomposites. *Cellulose* 2006; 13: 261–270.

46. Deepa B, Abraham E, Cherian BM, et al. Structure, morphology and thermal characteristics of banana nano fibers obtained by steam explosion. *Bioresour Technol* 2011; 102: 1988–1997.

47. Abral H, Ariksa J, Mahardika M, et al. Transparent and antimicrobial cellulose film from ginger nanofiber. *Food Hydrocolloid* 2020; 98: 105266.

48. Mahmoud KA, Mena JA, Male KB, et al. Effect of surface charge on the cellular uptake and cytotoxicity of fluorescent labeled cellulose nanocrystals. *ACS Appl Mater Interface* 2010; 2: 2924–2932.

49. Ilyas RA, Sapuan SM, Ibrahim R, et al. Production, processes and modification of nanocrystalline cellulose from agro-waste: a review. In: Movahedi B (ed.) *Nanocrystalline materials*. London, UK: IntechOpen, pp.3–32.

50. Naduparambath S, TVJ, Shaniba V, et al. Isolation and characterisation of cellulose nanocrystals from sago seed shells. *Carbohydr Polym* 2018; 180: 13–20.

51. Ramires EC and Dufresne A. A review of cellulose nanocrystals and nanocomposites. *Tappi J* 2011; 10: 9–16.

52. Ilyas RA, Sapuan SM, Atiqah A, et al. Sugar palm (Arenga pinnata [Wurmb.] Merr) starch films containing sugar palm nanofibrillated cellulose as reinforcement: water barrier properties. *Polym Compos* 2020; 41: 459–467.

53. Ilyas RA, Sapuan SM, Ibrahim R, et al. Effect of sugar palm nanofibrillated cellulose concentrations on morphological, mechanical and physical properties of biodegradable films based on agro-waste sugar palm (Arenga pinnata (Wurmb.) Merr) starch. *J Mater Res Technol* 2019; 8: 4819–4830.

54. Marett J, Aning A and Foster EJ. The isolation of cellulose nanocrystals from pistachio shells via acid hydrolysis. *Ind Crop Prod* 2017; 109: 869–874.

55. Flauzino Neto WP, Silvério HA, Dantas NO, et al. Extraction and characterization of cellulose nanocrystals

from agro-industrial residue – soy hulls. *Ind Crop Prod* 2013; 42: 480–488.

56. Alemdar A and Sain M. Biocomposites from wheat straw nanofibers: morphology, thermal and mechanical properties. *Compos Sci Technol* 2008; 68: 557–565.

57. AL-Oqla FM, Sapuan MS, Ishak MR, et al. Combined multi-criteria evaluation stage technique as an agro waste evaluation indicator for polymeric composites: date palm fibers as a case study. *BioResources* 2014; 9: 4608–4621.

58. AL-Oqla FM, Sapuan SM, Ishak MR, et al. A decision-making model for selecting the most appropriate natural fiber – polypropylene-based composites for automotive applications. *J Compos Mater* 2016; 50: 543–556.

59. Norizan MN, Abdan K, Ilyas RA, et al. Effect of fiber orientation and fiber loading on the mechanical and thermal properties of sugar palm yarn fiber reinforced unsaturated polyester resin composites. *Polimery* 2020; 65: 34–43.

60. Nurazzi NM, Khalina A, Sapuan SM, et al. Thermal properties of treated sugar palm yarn/glass fiber reinforced unsaturated polyester hybrid composites. *J Mater Res Technol* 2020; 9: 1606–1618.

61. Sanyang ML, Sapuan SM, Jawaid M, et al. Effect of sugar palm-derived cellulose reinforcement on the mechanical and water barrier properties of sugar palm starch biocomposite films. *BioResources* 2016; 11: 4134–4145.

62. Ilyas RA, Sapuan SM, Ishak MR, et al. Effect of delignification on the physical, thermal, chemical, and structural properties of sugar palm fibre. *BioResources* 2017; 12: 8734–8754.

63. Wise LE, Murphy M and D'Addieco AA. Chlorite, holocellulose, its fractionation and bearing on summative wood analysis and on studies on the hemicellulose. *Paper Trade J* 1946; 122: 35–43.

64. Segal L, Creely JJ, Martin AE, et al. An empirical method for estimating the degree of crystallinity of native cellulose using the X-Ray diffractometer. *Text Res J* 1959; 29: 786–794.

65. Chauve M, Barre L, Tapin-lingua S, et al. Evolution and impact of cellulose architecture during enzymatic hydrolysis by fungal cellulases. *Adv Biosci Biotechnol* 2013; 4: 1095–1109.

66. Yasim-Anuar TAT, Ariffin H, Norrrahim MNF, et al. Factors affecting spinnability of oil palm mesocarp fiber cellulose solution for the production of microfiber. *Bioresources* 2017; 12: 715–734.

67. Dufresne A. Nanocellulose: a new ageless bionanomaterial. *Mater Today* 2013; 16: 220–227.

68. Alemdar A and Sain M. Isolation and characterization of nanofibers from agricultural residues - wheat straw and soy hulls. *Bioresour Technol* 2008; 99: 1664–1671.

69. Nazrin A, Sapuan SM, Zuhri MYM, et al. Nanocellulose reinforced thermoplastic starch (TPS), polylactic acid (PLA), and polybutylene succinate (PBS) for food packaging applications. *Front Chem* 2020; 8: 1–12.

70. Ilyas RA, Sapuan SM, Ibrahim R, et al. Sugar palm (Arenga pinnata (Wurmb.) Merr) cellulosic fibre hierarchy: a comprehensive approach from macro to nano scale. *J Mater Res Technol* 2019; 8: 2753–2766.

71. Rosa MFM, Medeiros ES, Malmonge JAJ, et al. Cellulose nanowhiskers from coconut husk fibers: effect of preparation conditions on their thermal and morphological behavior. *Carbohydr Polym* 2010; 81: 83–92.

72. Phanthong P, Reubroycharoen P, Hao X, et al. Nanocellulose: extraction and application. *Carbon Res Convers* 2018; 1: 32–43.

73. Chan CH, Chia CH, Zakaria S, et al. Production and characterisation of cellulose and nano-crystalline cellulose from kenaf core wood. *BioResources* 2013; 8: 785–794.

74. Chowdhury ZZ and Hamid SBA. Preparation and characterization of nanocrystalline cellulose using ultrasonication combined with a microwave-assisted pretreatment process. *BioResources* 2016; 11: 3397–3415.

75. Mendes CAC, Ferreira NMS, Furtado CRG, et al. Isolation and characterization of nanocrystalline cellulose from corn husk. *Mater Lett* 2015; 148: 26–29.

76. Atikah MSN, Ilyas RA, Sapuan SM, et al. Degradation and physical properties of sugar palm starch / sugar palm nanofibrillated cellulose bionanocomposite. *Polimery* 2019; 64: 27–36.

77. Ray D and Sarkar BK. Characterization of alkali-treated jute fibers for physical and mechanical properties. *J Appl Polym Sci* 2001; 80: 1013–1020.

78. Mohanty AK, Misra M and Hinrichsen G. Biofibres, biodegradable polymers and biocomposites: an overview. *Macromol Mater Eng* 2000; 276–277: 1–24.

79. Lu P and Hsieh Y. Preparation and characterization of cellulose nanocrystals from rice straw. *Carbohydr Polym* 2012; 87: 564–573.

80. Frenot A, Henriksson MW and Walkenström P. Electrospinning of cellulose-based nanofibers. *J Appl Polym Sci* 2007; 103: 1473–1482.

81. Corrêa AC, de Morais Teixeira E, Pessan LA, et al. Cellulose nanofibers from curaua fibers. *Cellulose* 2010; 17: 1183–1192.

82. Wang Y, Wang G, Cheng H, et al. Structures of bamboo fiber for textiles. *Text Res J* 2010; 80: 334–343.

83. Talib RA, Tawakkal ISMA and Khalina A. The influence of mercerised kenaf fibres reinforced polylactic acid composites on dynamic mechanical analysis. *Key Eng Mater* 2011; 471–472: 815–820.

84. Hubbell CA and Ragauskas AJ. Effect of acid-chlorite delignification on cellulose degree of polymerization. *Bioresour Technol* 2010; 101: 7410–7415.

85. Pääkkö M, Vapaavuori J, Silvennoinen R, et al. Long and entangled native cellulose I nanofibers allow flexible aerogels and hierarchically porous templates for functionalities. *Soft Matter* 2008; 4: 2492.

86. Habibi Y and Vignon MR. Optimization of cellouronic acid synthesis by TEMPO-mediated oxidation of cellulose III from sugar beet pulp. *Cellulose* 2008; 15: 177–185.

87. de Morais Teixeira E, Bondancia TJ, Teodoro KBR, et al. Sugarcane bagasse whiskers: extraction and characterizations. *Ind Crop Prod* 2011; 33: 63–66.

88. Ng H-MM, Sin LT, Tee TT, et al. Extraction of cellulose nanocrystals from plant sources for application as

reinforcing agent in polymers. *Compos B Eng* 2015; 75: 176–200.

89. Kian LK, Jawaid M, Ariffin H, et al. Isolation and characterization of nanocrystalline cellulose from roselle-derived microcrystalline cellulose. *Int J Biol Macromol* 2018; 114: 54–63.

90. Guo J, Guo X, Wang S, et al. Effects of ultrasonic treatment during acid hydrolysis on the yield, particle size and structure of cellulose nanocrystals. *Carbohydr Polym* 2016; 135: 248–255.

91. Klemm D, Heublein B, Fink H-P, et al. Cellulose: fascinating biopolymer and sustainable raw material. *Angewandte Chemie Int Ed* 2005; 44: 3358–3393.

92. Vasconcelos NF, Feitosa JPA, da Gama FMP, et al. Bacterial cellulose nanocrystals produced under different hydrolysis conditions: properties and morphological features. *Carbohydr Polym* 2017; 155: 425–431.

93. Cherian BM, Leão AL, de Souza SF, et al. Isolation of nanocellulose from pineapple leaf fibres by steam explosion. *Carbohydr Polym* 2010; 81: 720–725.

94. Singh S, Gaikwad KK, Park S II, et al. Microwave-assisted step reduced extraction of seaweed (Gelidiella aceroso) cellulose nanocrystals. *Int J Biol Macromol* 2017; 99: 506–510.

95. Luzi F, Fortunati E, Puglia D, et al. Optimized extraction of cellulose nanocrystals from pristine and carded hemp fibres. *Ind Crop Prod* 2014; 56: 175–186.

96. Jiang Y, Zhou J, Zhang Q, et al. Preparation of cellulose nanocrystals from Humulus japonicus stem and the influence of high temperature pretreatment. *Carbohydr Polym* 2017; 164: 284–293.

97. Ilyas RA, Sapuan SM, Ibrahim R, et al. Thermal, biodegradability and water barrier properties of bio-nanocomposites based on plasticised sugar palm starch and nanofibrillated celluloses from sugar palm fibres. *J Biobase Mater Bioenerg* 2020; 14: 234–248.

98. Mandal A and Chakrabarty D. Isolation of nanocellulose from waste sugarcane bagasse (SCB) and its characterization. *Carbohydr Polym* 2011; 86: 1291–1299.

99. Wahono S, Irwan A, Syafri E, et al. Preparation and characterization of ramie cellulose nanofibers/CaCO3 unsaturated polyester resin composites. *ARPN J Eng Appl Sci* 2018; 13: 746–751.

100. Syafri E, Kasim A, Abral H, et al. Synthesis and characterization of cellulose nanofibers (CNF) ramie reinforced cassava starch hybrid composites. *Int J Biol Macromol* 2018; 120: 578–586.